ELSEVIER

Polymer 42 (2001) 8125–8135

polymer

www.elsevier.nl/locate/polymer

Ultra-drawing of low molecular weight polyethylene — ultra-high molecular weight polyethylene blend films prepared by gelation/crystallization from semi-dilute solutions

Yuezhen Bin, Lin Ma, Reiko Adachi, Hiromichi Kurosu, Masaru Matsuo*

Department of Textile and Apparel Science, Faculty of Life and Environment, Nara Women's University, Nara 630-8263, Japan

Received 9 February 2001; received in revised form 17 April 2001; accepted 23 April 2001

Abstract

Greatest drawability was studied for blend films with branched low molecular weight polyethylene (B-LMWPE) and ultra-high molecular weight polyethylene (UHMWPE) prepared by gelation/crystallization from solutions. The morphology of B-LMWPE–UHMWPE dry gel film and its deformation mechanism were mainly estimated by using differential scanning calorimeter, small-angle X-ray scattering, wide-angle X-ray diffraction and solid-state ^{13}C NMR. The detailed analysis was carried out for the blend films including large amounts of B-LMWPE. As a result, it was found that the UHMWPE and B-LMWPE were crystallized separately from the mixed solution. The greatest drawability was attributed to a suitable number of entanglements between UHMWPE crystal lamellae that are highly oriented with their large flat faces parallel to the film surface. These entanglements play an important role to transmit the drawing force as intermolecular cross-links and ensured smooth crystal transition of UHMWPE from a folded to a fibrous. In this process, large amount of B-LMWPE is thought to be almost independent of the ultra-drawing behavior of UHMWPE, since the domains of UHMWPE and B-LMWPE within the blend have no interaction and B-LMWPE crystallites take almost a random orientation. © 2001 Published by Elsevier Science Ltd.

Keywords: Greatest drawability of blend films; Branched low molecular weight polyethylene; Ultra-high molecular weight polyethylene

1. Introduction

Extensive investigations have been performed in new processing methods for obtaining high performance fiber of ultra-high molecular weight polyethylene (UHMWPE) [1–10]. Among these processing methods, ultra-drawing of specimens prepared by quenching of UHMWPE solutions and by drying the resultant gels has attracted attention in terms of its variable availability in the production of high strength and high modulus fiber commercially [1–5,7]. The gel-spun UHMWPE fibers have excellent mechanical properties with Young's modulus of 100–220 GPa and tensile strength of 3–6 GPa, respectively [9,11]. Such mechanical properties are ascribed to high crystallinity and fully extended crystal chains oriented with respect to the stretching direction.

Recently, low molecular weight polyethylene (LMWPE) with low viscosity has been carried out to prepare blends with UHMWPE to produce high modulus fibers [12-16]. As a result, it was confirmed that the possibility of the introduction of branched low molecular weight polyethylene (B-LMWPE) causes significant decrease in solution viscosity when total PE is fixed and promotes the high production rate. Interestingly, B-LMWPE–UHMWPE blend gel with 90% B-LMWPE content could form films and the resulting films could be elongated up to 200-fold [16], although B-LMWPE ($\bar{M}_v < 3 \times 10^5$) has no ability to form a film and they broke up into flakes during drying [13]. However, such a phenomenon as ensuring the greatest drawing has never been reported for linear low molecular weight polyethylene (L-LMWPE)–UHMWPW blends. This reason has been an unresolved problem.

In order to investigate the origin concerning high drawability of B-LMWPE–UHMWPE blend films, this paper is concentrated on the morphology of B-LMWPE–UHMWPE dry gel film and its deformation mechanism under the ultra-drawing. Experiments were mainly carried out for the blend films including large amounts of B-LMWPE, by using

* Corresponding author. Address: Division of Genetics, International Center for Medical Research, Kobe University School of Medicine, 7-5-1, Kusunoki-cho, Chuo-ku, Kobe, Hyogo 650, Japan. Tel. & fax: +81-742-20-3462.

E-mail addresses: m-matsuo@cc.nara-wu.ac.jp (M. Matsuo), matsuo@kobe-u.ac.jp (M.Matsuo).

0032-3861/01/$ - see front matter © 2001 Published by Elsevier Science Ltd.
PII: S0032-3861(01)00302-0

differential scanning calorimeter (DSC), small-angle X-ray scattering (SAXS), wide-angle X-ray diffraction (WAXD) and solid-state ^{13}C NMR.

2. Experimental

2.1. Specimen preparation

The materials used in the present work were B-LMWPE (Sumikathen G808) with a viscosity-average molecular weight ($\bar{M}_v$) of 2.07×10^4, L-LMWPE (Sholex super 4551H) with $\bar{M}_v = 2.84 \times 10^5$ and UHMWPE (Hercules 1900/90198) with $\bar{M}_v = 6 \times 10^6$. Specimens were prepared by gelation/crystallization from solutions by quenching the solutions well mixed at 135°C to room temperature. Solvent was decalin. The compositions of B-LMWPE and UHMWPE chosen were 0/1, 1/1, 2/1, 4/1, 9/1 and 1/0. The concentration of UHMWPE was fixed to be 0.4 g/100 ml against solvent and the amount of B-LMWPE was determined as relative ratio to UHMWPE. For example, the 9/1 composition corresponds to 3.6 g of B-LMWPE and 0.4 g of UHMWPE in 100 ml decalin. The dry gel films were cut into strips of 30 mm length and 10 mm width. The specimens were elongated manually up to desired ratios at 135°C and then quenched at room temperature. The details about the preparation of samples were described previously [16]. Incidentally, L-LMWPE–UHMWPE blend films were prepared for the 9/1 composition by using the same method.

2.2. Experimental procedures

The calorimetric investigations of dry gel films and their drawn specimens were performed on a Rigaku Thermoflex TG8110 apparatus with TG–DSC mode at a heating rate of 5°C min^{-1}. The weight of specimen was 5 mg. The crystallization and solubility of gels containing large amount of decalin were measured with an Exstar 6000 of Seiko Instrument using decalin as reference. The heating and cooling rate was 1°C min^{-1}. Densities of the specimens were measured by a pycnometry using a mixture of chlorobenzene and toluene at 20°C. The detailed estimation was described elsewhere [11]. The crystal weight fraction (crystallinity) within the blends was also computed from DSC curves by assuming the heat of fusion at equilibrium melting temperature of fully crystalline PE to be 286.8 J g^{-1} [17].

Young's modulus and tensile strength for the specimens were measured with an Instron tensile testing machine. The initial dimensions of specimens were: length, 60 mm; width, 2 mm. The distance between two metallic clamps, corresponding to the length of the specimens to be drawn, was fixed as 20 mm. The specimens were elongated at the cross-head speed of 2 mm min^{-1} at room temperature.

The X-ray pattern and intensity distribution were obtained by using a 12 kW rotating anode X-ray generator (Rigaku RDA-rA operated at 200 mA and 40 kV) and X-ray beam with Cu Kα radiation was monochromatized using a curved graphite monochromator. The estimation by SAXS, WAXD and complex dynamic moduli is described in detail elsewhere [18,19].

High-resolution solid-state ^{13}C NMR measurements were performed at room temperature on a JEOL JM-EX270 spectrometer at a ^{13}C frequency of 67.8 MHz. The magic-angle spinning rate was 5–5.5 kHz. The contact time in ^{13}C CP/MAS measurement was 2 ms. The chemical shift relative to tetramethylsilane (Me_4Si) was determined from the higher field signal (29.5 ppm) of adamantine. Spin–lattice relaxation time (T_{1C}) was measured by T1CP pulse sequence developed by Torchia [20].

3. Results and discussion

The drawability of the gel specimens was dependent principally upon the concentration of the solution from which the gel was made [12,13,21]. The achievable draw ratio of the UHMWPE gel film reached more than 300-fold, when they were prepared near their critical (optimum) concentrations. However, the achievable drawability reduced significantly as the solution concentration deviated from their critical values. This phenomenon is attributed to a reduced number of entanglements per molecule in the solution. In accordance with previous works [22,23], the solution at the critical concentration maintains a suitable level of entanglements between crystal lamellae within the resultant dry film after evaporation of solvents and the entanglements play an important role to transmit the drawing force as intermolecular cross-links. Consequently, the greatest drawability up to 300-fold can be achieved by the transformation from folded to fibrous crystals. Yeh et al. [12] studied the change of critical concentration of UHMWPE and B-LMWPE blend in decalin solution and its influence on the maximum draw ratio in detail. According to their paper, the critical concentration was varied from 0.70 to 1.3 g/100 ml for the specimens with 100/0 and 70/30 compositions, respectively. They pointed out that the critical concentration reduces slightly, since the presence of B-LMWPE in blend film reduces the number of inter- and intra-molecular entanglements between UHMWPE chains. Accordingly, the maximum draw ratio increases by introducing less than 5% B-LMWPE into UHMWPE. However, the draw ratios reduce considerably when B-LMWPE content was beyond 20%.

In our experiment, the viscosity of polyethylene solutions was measured with the Ubbelohde type capillary viscometer at 135°C. The relationship between viscosity of solution at 135°C and content of B-LMWPE in the blends is shown in Fig. 1. UHMWPE against solvent was fixed to be 0.4 g/100 ml, corresponding to the critical concentration for UHMWPE homo-polymer solutions in decalin [22,23]. Hence, the total concentration of the solutions increases with increasing B-LMWPE content. The profile indicates

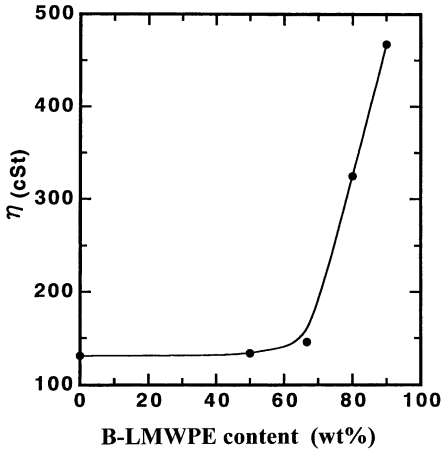

Fig. 1. Relationship between viscosity of B-LMWPE and UHMWPE mixed solution as a function of B-LMWPE content, in which UHMWPE concentration was fixed at 0.4 g/100 ml.

that the viscosity of blend solution is nearly equal to that of UHMWPE solution when the content of B-LMWPE is less than 67% (B-LMWPE/UHMWPE = 2/1) of total PE in the solution. The dry gel films with 1/1 and 2/1 compositions could be elongated up to 200-fold easily as in the case of UHMWPE dry gel film. The viscosity of solution increases drastically when B-LMWPE content is beyond 67% and drawability up to 200-fold of the resultant dry films became worse. However, careful drawing could achieve elongation up to 200-fold for B-LMWPE–UHMWPE blends even containing 90% B-LMWPE. This result is quite different result from the results by Yeh et al. [12].

In order to investigate the origin concerning high drawability, the L-LMWPE and UHMWPE blend with 9/1 composition was also prepared by gelation/crystallization using the same method as B-LMWPE–UHMWPE blends. The concentration of UHMWPE was also 0.4 g/100 ml decalin. L-LMWPE gels had no ability to form a film and they broke into flakes during drying as B-LMWPE did [13]. The resultant dry blend of L-LMWPE–UHMWPE took a sponge-like structure. Of course, the sponge-like blend can form a hard bulk after being pressed under 5 MPa press at room temperature. Even so, the film could not be elongated more than fivefold at any elongation condition.

Fig. 2 shows the temperature dependence of storage and loss moduli for the two kinds of 9/1 blends. The specimen of L-LMWPE–UHMWPE was pressed at room temperature. The storage modulus of B-LMWPE–UHMWPE blend is much higher than that of L-LMWPE–UHMWPE blend at temperatures < -20°C. For the loss modulus, the considerable β-relaxation was observed for B-LMWPE–UHMWPE blend in the temperature range of −40–40°C. This behavior is found to be characteristic of the storage and loss moduli of B-LMWPE melt films with low crystallinity. Judging from the same composition of 9/1, the storage and loss moduli of the blends are strongly affected by the intrinsic mechanical properties of B-LMWPE and L-LMWPE. For the L-

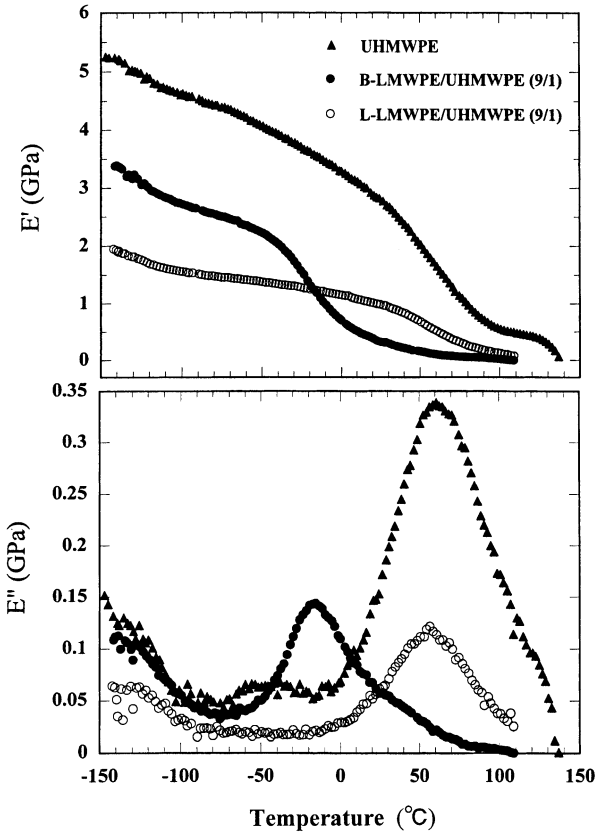

Fig. 2. Temperature dependence of the storage and loss moduli of B-LMWPE–UHMWPE (9/1), L-LMWPE–UHMWPE (9/1) and UHMWPE films in undrawn state.

LMWPE–UHMWPE blend, not β-relaxation but α-relaxation could be observed significantly [18]. The storage and loss moduli of the L-LMWPE–UHMWPE blend was confirmed to show similar profile to those of UHMWPE, although the magnitude of the storage modulus is lower. The storage and loss moduli of the B-LMWPE–UHMWPE dry gel film were similar to those of B-LMWPE melt film.

SAXS patterns (end view) for all the B-LMWPE–UHMWPE blends and the L-LMWPE–UHMWPE blends (9/1) show the meridional scattering maxima, as has been observed for the UHMWPE film. The scattering arcs became longer with increasing B-LMWPE (and L-LMWPE) content reflecting an increase in orientation fluctuation of crystal lamellae to the film surface. To shorten the paper, the patterns are not shown in this paper. The detailed analysis was done from SAXS intensity distributions as a function of scattering angle $2\theta_B$ in the meridional direction by using a position sensitive proportional counter (PSPC) system. Fig. 3(a) and (b) shows the results. As shown in column (a), the scattering maxima become more indistinct as B-LMWPE content increases. This indicates that the dry gel films are composed of highly oriented crystal lamellae with their flat face parallel to the film surface but the orientational fluctuation of crystal lamellae becomes more pronounced with increasing B-LMWPE content. On the

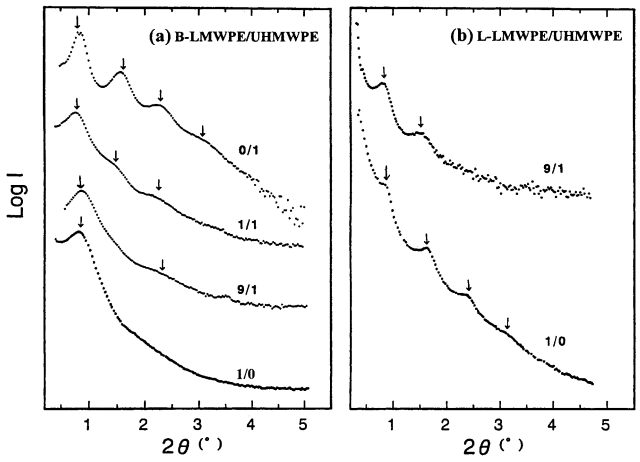

Fig. 3. SAXS intensity distributions for the undrawn blends in the meridional direction by PSPC system: (a) B-LMWPE–UHMWPE; (b) L-LMWPE–UHMWPE.

other hand, the profiles in column (b), L-LMWPE dry gel shows the fourth-order scattering, while the blend gel film of L-LMWPE–UHMWPE (9/1) shows the second-order scattering maximum. Comparing the distribution curve of the B-LMWPE with that of the 9/1 blend, the higher order peaks of the 9/1 blend become less distinct. This result also supports that the UHMWPE hampers the orientation of B-LMWPE crystal lamellae oriented parallel to the film surface.

The periodic distance L of lamellae estimated from the profiles of SAXS intensity distributions is listed in Table 1. The value of L becomes smaller slightly by introduction of B-LMWPE but it is not influenced greatly. As discussed before, the viscosity of solutions to prepare the 1/1 (50%) and 2/1 (67%) blend gels was almost the same as that in the case of UHMWPE solution with 0.4 g/100 ml. By introducing B-LMWPE content higher than 67%, the viscosity increases drastically. In this case, although the isolated UHMWPE chains also form large crystal lamellae under the gelation, the crystal lamellae cannot orient significantly parallel to the film surface. This is thought to be due to the fact that large amounts of B-LMWPE hamper the ordered orientation of the UHMWPE lamellae.

Further attention was focused on a quantitative estimation of the boundary (transition) regions corresponding to folded loops on the basis of SAXS intensity distribution at $2\theta = 4.5$–$8.0°$ higher than the scattering angle shown in Fig. 3(a). On subtracting the background scattering corresponding to the amorphous and thermal diffuse scattering from the total scattered intensity, the background scattering was approximated as a straight line. Through trial and error, it was found that the manner of subtracting the background scattering did not much affect the final value of the density fluctuation at the interface.

Table 1
The long period L and the interface thickness t of gel film with different compositions

B-LMWPE/UHMWPE	L (Å)	t (Å)
0/1	111.5	10.2
1/1	110.4	10.3
2/1	110.4	10.9
4/1	107.2	11.2
9/1	106.6	11.6

The system to be considered here is the one that has one-dimensional electron density fluctuation along a direction normal to the lamellar interfaces and the density variation is periodic [24–26]. Namely, this system composes of disk-like crystal lamellae parallel to the film surface. The variation deviates from an ideal two-phase system in which the density variation occurs discontinuously from electron density of crystal lamellae and voids.

If the electron density variation is given by a Gaussian function, the scattered intensity $I(s)$ at larger angle tails, corrected for background scattering, is given by [5]

$$I(s) = (\text{const})s^{-2} \exp(-4\pi^2\sigma^2 s^2) \quad (1)$$

where

$$s = \frac{2 \sin \theta}{\lambda}$$

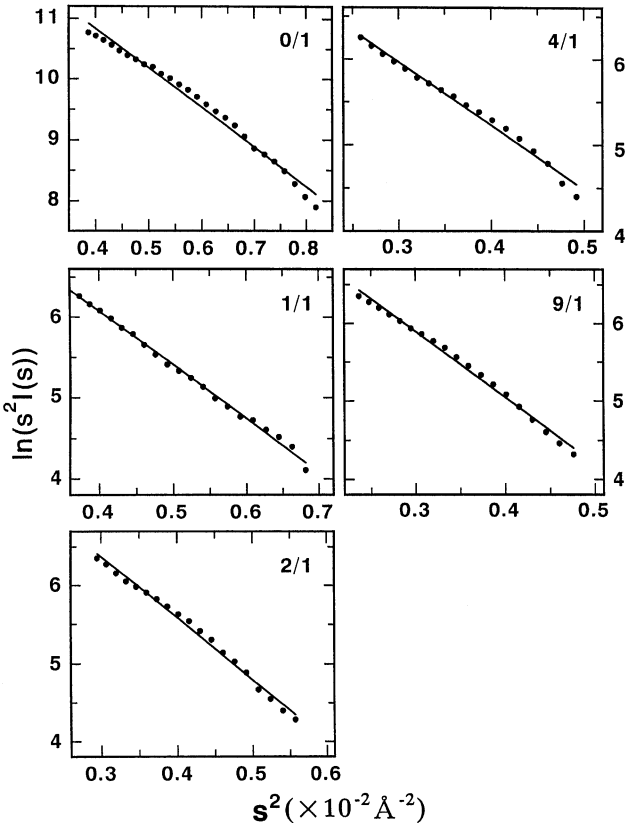

Fig. 4. $\ln(s^2 I(s))$ vs. s^2 of blend gel films with the indicated compositions.

where λ is the wavelength of X-ray and 2θ the scattering angle.

Fig. 4 shows the relationship between $I(s)$ and s^2 for dry gel films with different compositions (B-LMWPE/UHMWPE = 0/1–9/1). σ is the parameter denoting standard variation characterizing the diffuseness of boundary, and it is associated with the interfacial thickness t, as follows:

$$\sigma = (2\pi)^{-1/2} t \quad (2)$$

The value σ can be evaluated from the slope in the plot of $\ln(s^2 I(s))$ vs. s^2. The values of the interfacial thickness t calculated from above equation are listed in Table 1. With increasing B-LMWPE content, the long period L decreases slightly and the interfacial thickness t increases. An increase in t leads to a decrease in crystal lamellar thickness and a drop of melting point as discussed later (see Fig. 6). But the variances of L and t are not so large. This indicates that the introduction of large amounts of B-LMWPE does not influence greatly the formability of crystal lamellae of UHMWPE. Of course, the plots of $\ln(s^4 I(s^4))$ vs. s^4 associated with a random system [26] were confirmed to deviate from a linear relationship in preliminary experiments.

To check the results in Table 1, DSC measurements were done and the results are shown in Figs. 5 and 6. Fig. 5 shows the DSC curves of L-LMWPE dry gels and L-LMWPE–UHMWPE (9/1 composition) dry gel film. A single endotherm peak appears indicating the co-crystallization of L-LMWPE and UHMWPE by quenching the solution. The peak of the blend becomes a little bit sharper than that of UHMWPE and heat of fusion becomes also higher, but the melting point is hardly affected by the introduction of UHMWPE.

Fig. 6 shows the DSC curves for B-LMWPE–UHMWPE. Two endotherm peaks appear clearly for all B-LMWPE–UHMWPE blend gel films. Judging from the curves of two homo-polymers of B-LMWPE (1/0 composition) and UHMWPE (0/1 composition), it is evident that the peak

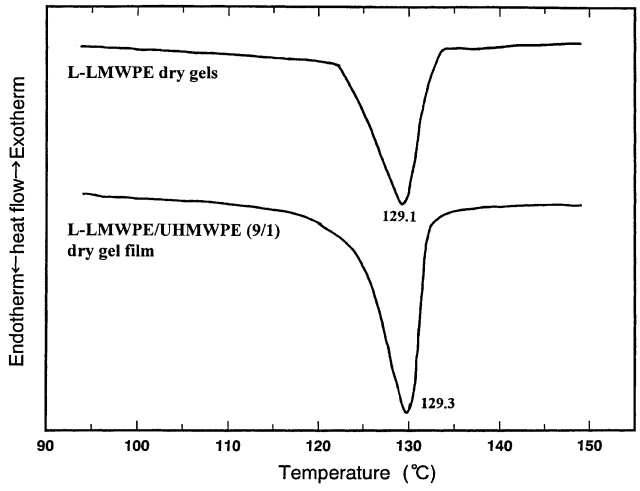

Fig. 5. DSC curves of undrawn L-LMWPE dry gels and L-LMWPE–UHMWPE blend gel films with 9/1 composition.

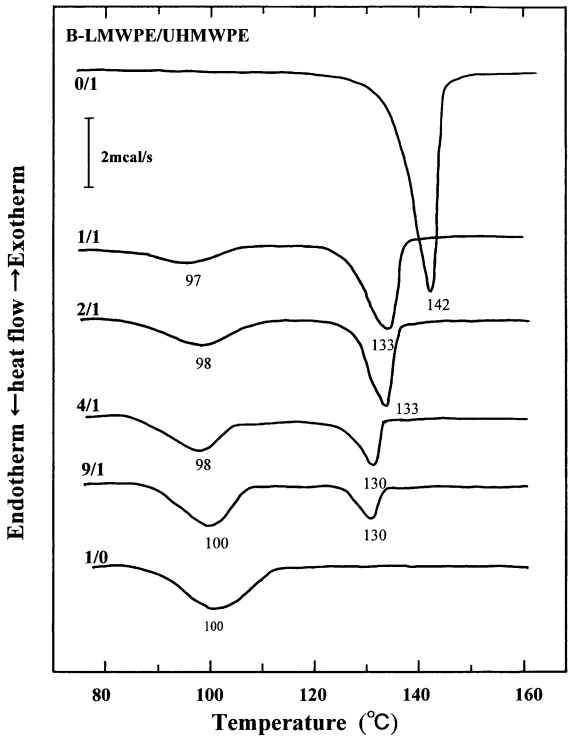

Fig. 6. DSC curves for undrawn B-LMWPE–UHMWPE dry gel films with various compositions.

on lower temperature side (97–100°C) corresponds to melting of B-LMWPE crystallites, while the peak on higher temperature side (130–133°C) corresponds to melting of UHMWPE crystallites. The melting point of UHMWPE crystallites within the blend is much lower than the melting point of UHMWPE homo-polymer gel film. In spite of small difference of L and t in Table 1, the drastic decrease in the melting point of UHMWPE indicates that UHMWPE crystallites within the blend are in unstable state containing a number of voids and this tendency becomes more pronounced with increasing B-LMWPE content. In contrast, the melting points on the low temperature were hardly affected by B-LMWPE content. Appearance of the two separated peaks indicates obviously that B-LMWPE and UHMWPE are crystallized separately by quenching the mixed solution and the crystal growth under the evaporation of the solvent is also progressive separately.

To obtain further confirmation, DSC measurements were also carried out for gels containing decalin obtained by quenching solution from 135°C. Fig. 7(a) and (b) shows the curves of B-LMWPE–UHMWPE (9/1) and L-LMWPE–UHMWPE (9/1) gels under cooling and heating process, in which decalin was adopted as reference. Under the cooling process, it is obvious that L-LMWPE is co-crystallized with UHMWPE showing a single exotherm peak at 76.8°C. For the B-LMWPE–UHMWPE system, another broad peak at 36.6°C appeared in cooling process and enthalpies calculated from the peaks on the lower and higher sides were 11.1 and 1.4 J g^{-1}, respectively. In the heating

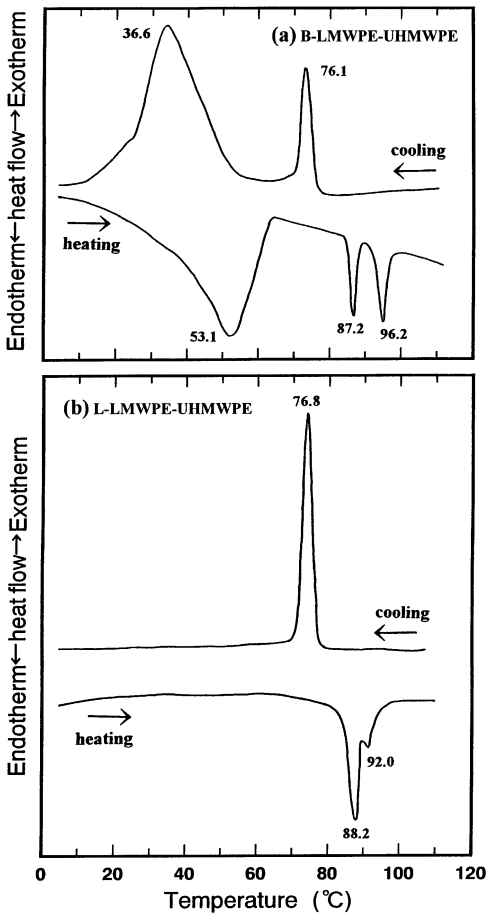

Fig. 7. DSC curves in the heating and cooling processes for gels containing a lot of decalin with 9/1 composition: (a) B-LMWPE–UHMWPE; (b) L-LMWPE–UHMWPE.

process, the endotherm peak on the lower temperature side appears at 53.1°C for the B-LMWPE–UHMWPE gels, while there is no peak below 70°C for the L-LMWPE–UHMWPE gels. Through the results, it was confirmed that B-LMWPE and UHMWPE are crystallized separately by quenching the mixed solution.

In the B-LMWPE–UHMWPE (9/1) solutions, long UHMWPE chains, which are isolated from short B-LMWPE chains, are thought to consist of interpenetrating random coils forming a suitable level of their entanglements. The entanglements are maintained within the dry gel film and act as inter-lamellar cross-links, which effectively transmit the drawing force. Short molecular chains of B-LMWPE form a number of small folded chain crystals but do not form entanglements with UHMWPE chains. Accordingly, ultra-drawing of B-LMWPE–UHMWPE up to $\lambda = 200$ is essentially similar to that of UHMWPE. Namely, a suitable level of the entanglements of UHMWPE ensures the crystal transition from a folded to a fibrous type in order to realize the high drawability.

In contrast, the L-LMWPE–UHMWPE in the mixed solution were co-crystallized and within the resultant film, there exist entanglements between L-LMWPE and UHMWPE chains besides crystal lamellae with various sizes. The lamellae formed by co-crystallization of L-LMWPE and UHMWPE hamper the smooth crystal transition of UHMWPE from folded to fibrous type. In some places within the specimen, stress concentration within the blend occurs as has been confirmed for drawing of melt films. Actually, the 9/1 blends could not be drawn to more than fivefold.

The melting points, heat of fusion and crystallinity for the blends with various compositions are summarized in Table 2 from the results of DSC measurements in Fig. 6. Crystallinity estimated from density measurements is also listed here. The crystallinity by the density measurements is higher than that of from DSC measurement for all the specimens. The systematic difference between the two methods is thought to relevant to the presence of an intermediate phase as suggested by Mandelkern and coworkers [27,28] for melt-crystallized as well as for solution-crystallized polyethylene and ethylene copolymers. Notwithstanding this fact, the crystallinity increases with decreasing the content of B-LMWPE from both measurements.

Fig. 8 shows the change in crystallinity estimated by DSC for the B-LMWPE and UHMWPE within the blend as a function of B-LMWPE content. 'Total' is the crystallinity of the specimens. Each heat of fusion was calculated by the relationship: heat of fusion = observed value/content of

Table 2
Melting point T_m, heat of fusion H_u, density ρ and crystallinity X_c of undrawn B-LMWPE–UHMWPE blends

LMWPE/UHMWPE (LMWPE content (%))	Result from DSC						Result from density	
	Low temperature side		High temperature side		Total		ρ (g cm^{-3})	X_c (%)
	T_m (°C)	H_u (J g^{-1})	T_m (°C)	H_u (J g^{-1})	H_u (J g^{-1})	X_c (%)		
0/1 (0)	–	–	142	236.26	236.26	82.4	0.974	84.9
1/1 (50)	97	32.21	133	116.31	148.52	51.8	0.944	66.4
2/1 (67)	98	47.17	133	81.70	128.87	44.9	0.927	55.4
4/1 (80)	98	66.12	130	46.50	112.62	39.3	0.922	52.1
9/1 (90)	100	73.48	130	24.16	97.64	34.0	0.917	48.7
100/0 (100)	100	90.36	–	–	90.36	31.5	0.913	46.0

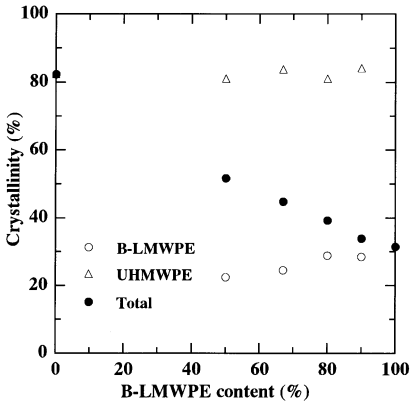

Fig. 8. Crystallinity against B-LMWPE content within B-LMWPE–UHMWPE blend films calculated from the heat of fusion.

UHMWPE (or B-LMWPE) and the crystallinity was estimated from the calculated heat of fusion. The crystallinity of UHMWPE is almost independent of B-LMWPE content within the blend films. In contrast, the crystallinity of B-LMWPE within the blend increases slightly as B-LMWPE content increases. Here, it should be noted that crystallinity of UHMWPE was almost independent of B-LMWPE content but the introduction of B-LMWPE slightly hampers the growth of large lamellar crystals of UHMWPE. The obstruction of the crystal growth supports the X-ray results shown in Table 1. It is well known that the equilibrium melting point is related to the thickness of lamellae and surface energy. It may be considered that shift of melting point of UHMWPE is associated with the decrease in lamellae thickness and increase in surface energy.

As discussed above, B-LMWPE–UHMWPE blend films prepared by crystallization from solution are possessed of a similar microstructure to UHMWPE gel films. The drawability is attributed to the long molecular chains of UHMWPE forming the large crystal lamellae and keeping a suitable level of entanglements between the lamellae. These entanglements transmit effectively the draw force in the stretching direction. Even so, it is very surprised that even the 9/1 blend could be stretched to more than 200-fold.

Now, we mainly discuss the mechanical properties and morphology of ultra-drawn films of B-LMWPE–UHMWPE blends. Young's modulus and tensile strength measured from an Instron tester as a function of draw ratios are listed in Table 3. All the data are average values measured for three or four pieces of the same sample. The values increase with increasing the draw ratio for all the specimens. However, the values of the blend films are much lower than those of UHMWPE homo-polymer at the same draw ratio. The reduction of Young's modulus and tensile strength is much more considerable in comparison with the decrease in UHMWPE content within blends. For the UHMWPE film at $\lambda = 200$, Young's modulus was more than 180 GPa. On the other hand, Young's modulus of the 9/1 blend was less than 10 GPa at the same draw ratio. The values of the 9/1 blend did not reach 1/20 of that of pure

Table 3
Young's modulus, E (GPa), and tensile strength, s (GPa), of B-LMWPE–UHMWPE blend films at various draw ratios

λ	B-LMWPE/UHMWPE				
	0/1	1/1	2/1	4/1	9/1
Young's modulus, E (GPa)					
10	15.8	2.36	2.16	1.12	0.70
20	42.58	7.18	3.22	3.20	1.84
50	69.26	12.08	8.18	7.82	2.36
100	104.36	23.68	12.64	11.23	4.96
200	187.12	66.72	14.82	13.18	8.56
Tensile strength, s (GPa)					
10	0.54	0.08	0.074	0.046	0.024
20	2.02	0.19	0.125	0.106	0.034
50	3.36	0.46	0.187	0.167	0.073
100	4.01	0.86	0.484	0.353	0.094
200	5.61	1.26	0.846	0.604	0.130

UHMWPE. This indicates that most of B-LMWPE crystallites are maintained folded type without the crystal transition to fibrous textures and they do not undertake the same amount of loads as UHMWPE molecular chains in the drawing process. As shown in the previous paper [16], the WAXD patterns of the 1/1 blend indicated that the c-axes of UHMWPE and B-LMWPE are highly oriented with respect to the stretching direction corresponding to the strong equatorial reflection spots as $\lambda > 100$ as that of UHMWPE at the same draw ratio. Young's modulus, however, was only about 36% of that of UHMWPE film with $\lambda = 200$.

Returning to Fig. 2, it may be noted that the temperature dependence of E'' of the L-LMWPE–UHMWPE (9/1) is similar to that of the UHMWPE, while the behavior of the B-LMWPE–UHMWPE is similar to that of B-LMWPE. This means that the crystallites and the amorphous phase of the B-LMWPE exist without any correlation with those of UHMWPE. Accordingly, as listed in Table 3, the very low Young's modulus <10 GPa of the 9/1 blend at $\lambda = 200$ is due to only the contribution of the extended crystal chains of the 10% UHMWPE and the rest 90% B-LMWPE plays as fillers. Namely, the B-LMWPE crystallites take a random orientation and are independent of the rise of Young's modulus in bulk. Following DSC, X-ray and ^{13}C NMR measurements are carried out to justify this assumption.

Fig. 9 shows the change in DSC curves of B-LMWPE–UHMWPE films with 9/1 composition at the indicated draw ratios. Table 4 lists the values of heat of fusion calculated from the area of the separated peaks. As a draw ratio increases up to 200-fold, the endotherm peak on high temperature side corresponding to melting of UHMWPE crystallites shifts from 130 to 134°C. The shifting degree of the melting point is much smaller than UHMWPE homopolymer gel films [29]. Incidentally, for the UHMWPE film with draw ratio > 100, the melting point increased more than 10°C reflecting drastic oriented crystallization [29]. On the other hand, the endotherm peak at lower temperature side corresponding to melting of B-LMWPE was hardly

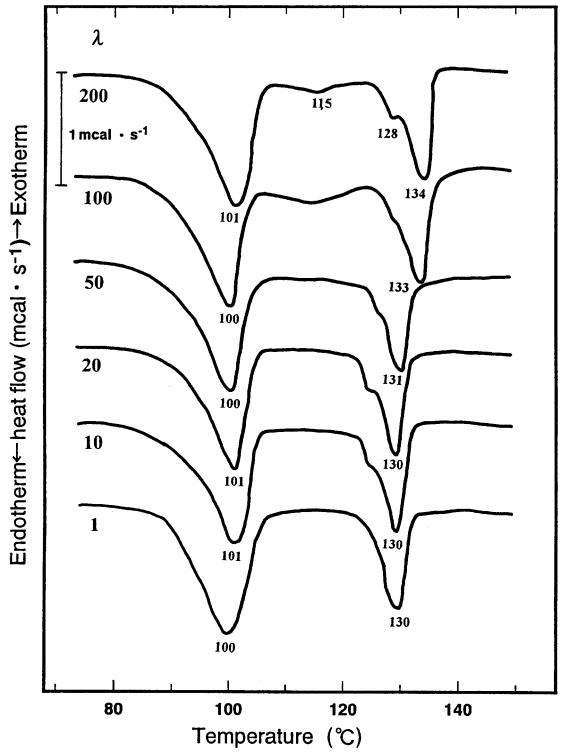

Fig. 9. DSC curves as a function of draw ratio measured for B-LMWPE–UHMWPE dry gel films with 9/1 composition.

influenced by elongation. Anyway, the peak areas of the both peaks are hardly affected by elongation, indicating no significant growth of crystallites and no increase in crystallinity by oriented crystallization.

In order to facile understanding, the thermal stability of B-LMWPE and UHMWPE crystallites, WAXD measurement was carried out to check heat resistance of the B-LMWPE and UHMWPE crystallites. The specimens were fixed at a constant stress of 0.5–5 MPa to avoid the shrinkage of the films. The desirable stress was controlled at different temperature. The samples were annealed for 10 min at the indicated temperature prior to photographing. Fig. 10 shows the WAXD patterns from B-LMWPE–UHMWPE (9/1) blend films with $\lambda = 50$ and 200 measured at various temperatures. Pattern (a) shows that different orientation modes of B-LMWPE and UHMWPE crystallites co-existed within the both samples with $\lambda = 50$ and 200. It is obvious that the diffraction ring from the (110) plane is attributed to the orientation of B-LMWPE crystallites and the sharp diffraction spots are due to the orientation of UHMWPE crystallites. This supports the results in Table 3 that Young's modulus decreased with increasing B-LMWPE content. Namely, for the specimens with $\lambda = 200$, Young's modulus of the UHMWPE film is beyond 180 GPa while that of the B-LMWPE–UHMWPE (9/1) film is lesser than 10 GPa. In spite of an increase in draw ratio from 50- to 200-fold, the orientation of most of B-LMWPE crystallites within the blend film takes a random mode without significant improvement by further elongation.

In patterns (b)–(d), it is seen that the diffraction intensity for specimen with $\lambda = 50$ reduces faster than that with $\lambda = 200$ as the temperature increases. At 150°C, the B-LMWPE crystallites with a random orientation and UHMWPE crystallites with high orientation were melted perfectly for the specimen with $\lambda = 50$ but the reflection spots of UHMWPE crystallites slightly remain for the specimens with $\lambda = 200$.

To obtain more quantitative result for temperature dependence of the crystallites, temperature dependence of WAXD diffraction intensity distribution from the (002) plane was measured for the specimen with $\lambda = 200$ as a function of the composition. The measurement was carried out with a point focusing with a system in which an incident beam was collimated by a collimator 2 mm in diameter, and the diffraction beam was measured by a square slit of 0.9 mm × 0.9 mm. Scanning was performed on the equator in the 2θ range of 72.5–77.5°. The diffraction intensity distribution was measured with a step-scanning device with a step of 0.1°, with time interval of 100 s. Fig. 11(a) and (b) shows the results of the (002) plane measured for UHMWPE and B-LMWPE–UHMWPE blend with 9/1 composition, respectively.

In parts (a) and (b), the samples with nearly same thickness were selected as the test specimens. The intensity distributions were corrected for air scattering. The peak intensity of the (002) for the 9/1 blend is almost about 12% of the peak intensity for UHMWPE at 25°C. Nevertheless, the intensity ratio is just a little bit higher than the

Table 4
The change of melting point T_m, heat of fusion H_u, density ρ and crystallinity X_c of B-LMWPE–UHMWPE (9/1) blends under ultra-drawing

Draw ratio, λ	Result from DSC						Result from density	
	Low temperature side		High temperature side		Total		ρ (g cm^{-3})	X_c (%)
	T_m (°C)	H_u (J/g^{-1})	T_m (°C)	H_u (J/g^{-1})	H_u (J/g^{-1})	X_c (%)		
1	100	73.48	130	24.16	97.64	34.0	0.917	48.7
10	101	56.54	130	25.02	81.56	28.4	0.918	49.4
20	101	54.47	130	25.56	80.03	27.9	0.919	50.1
50	100	51.08	131	24.96	76.04	25.9	0.920	50.7
100	100	50.34	133	23.99	74.33	25.4	0.920	50.7
200	101	49.02	134	23.27	72.29	25.2	0.921	51.4

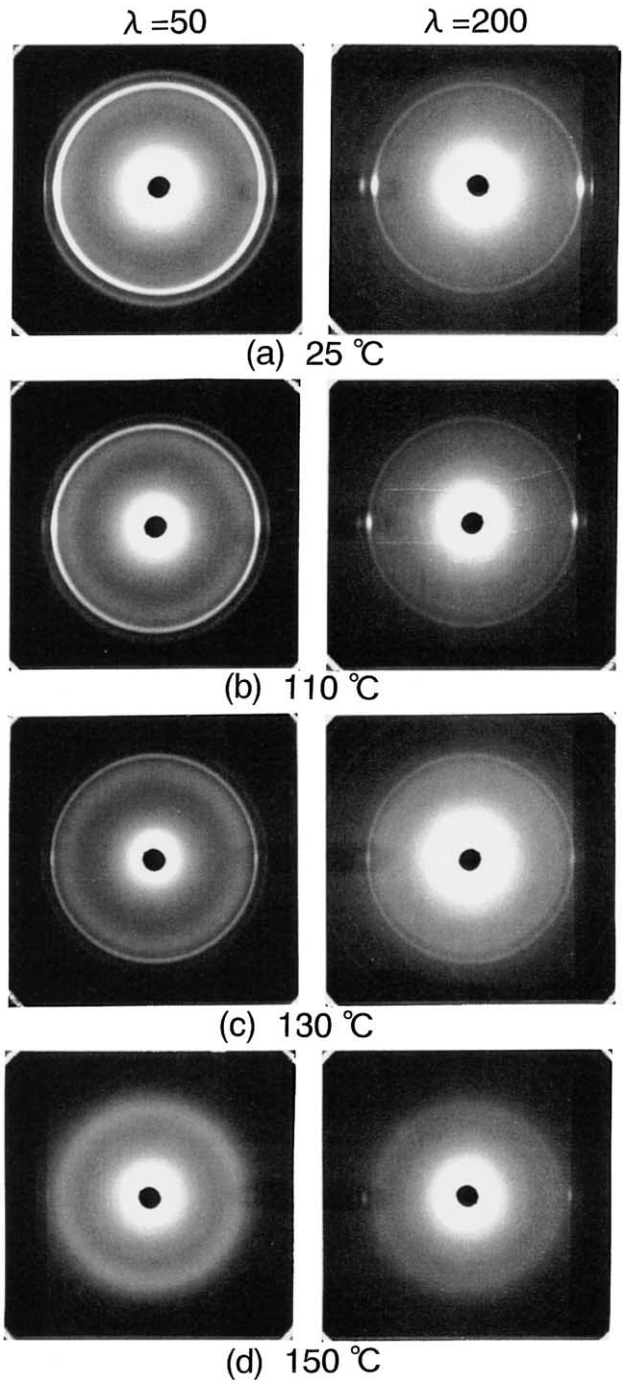

Fig. 10. WAXD patterns for B-LMWPE–UHMWPE (9/1) blends $\lambda = 50$ and 200 observed at various temperatures.

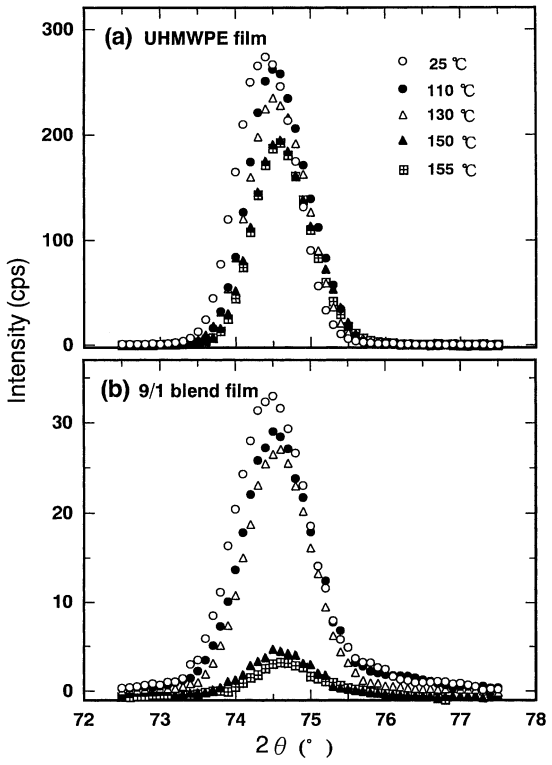

Fig. 11. WAXD diffraction intensity distribution of gel films with $\lambda = 200$ at various temperatures: (a) UHMWPE film; (b) B-LMWPE–UHMWPE (9/1) blends.

weight ratio of UHMWPE to B-LMWPE. Anyway, the lower peak intensity for the 9/1 blend is thought to be due to two possibilities: (1) lower crystallinity of B-LMWPE and (2) poor orientation of B-LMWPE crystallites with respect to the stretching direction. The intensity for the UHMWPE in part (a) only decreases about 30% at 155°C higher than the equivalent melting point of polyethylene. On the other hand, the intensity for the 9/1 blend in part (b) decreases slowly with increasing temperature up to 130°C but reduces drastically beyond 130°C. The intensity at 155°C is about 23% of that at 25°C. It is of interest to consider that the decrease in diffraction intensity in the range of 130–150°C is attributed to the melting of B-LMWPE component and the broad diffraction peak in part (b) at 155°C is attributed to the diffraction from small amount of UHMWPE crystallites. At 155°C, the peak intensity from UHMWPE film is about 80 times than that from B-LMWPE–UHMWPE blend. This is probably due to the fact that the UHMWPE crystallites within the 9/1 blend film are smaller and in more unstable state in comparison with those within the UHMWPE homo-polymer film. This indicates that the existence of large amounts of B-LMWPE hampers the perfect crystal transformation from a folded to fibrous type of UHMWPE crystallites.

Fig. 12 shows that ^{13}C CP/MAS spectra for the UHMWPE films and the 9/1 blends with $\lambda = 1$ and 200. The CP/MAS spectra emphasize the contribution of the crystalline phase. All the spectra were analyzed by least-squares fitting on the basis of the assumption of a superposition curve of Gaussian and Lorentzian functions. These spectra are shown to explain the outline of different characteristics between UHMWPE and B-LMWPE–UHMWPE films roughly. In this process, the line width and the peak height of each component were determined to give the best fit by computer on the basis of small changes from the initial peak position. The initial values of all the components were given by adopting the corresponding chemical shifts of

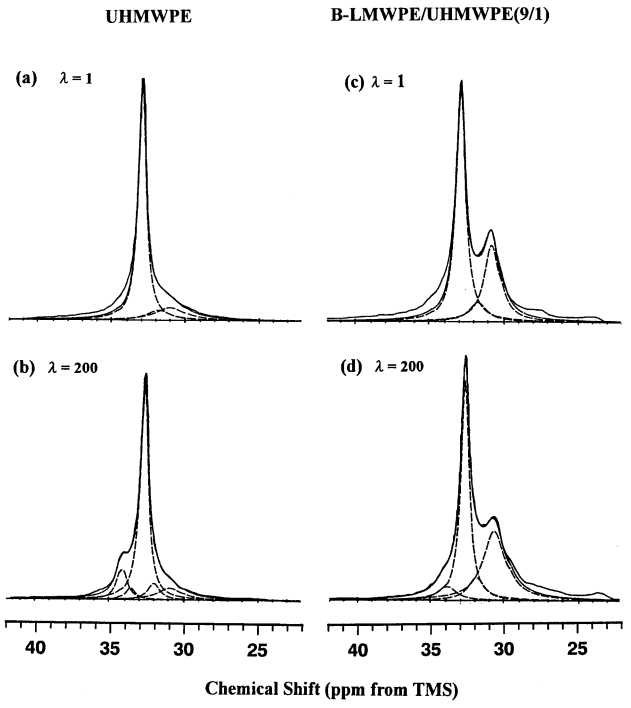

Fig. 12. ^{13}C CP/MAS spectra of UHMWPE films and B-LMWPE–UHMWPE (9/1) blend with $\lambda = 1$ and 200.

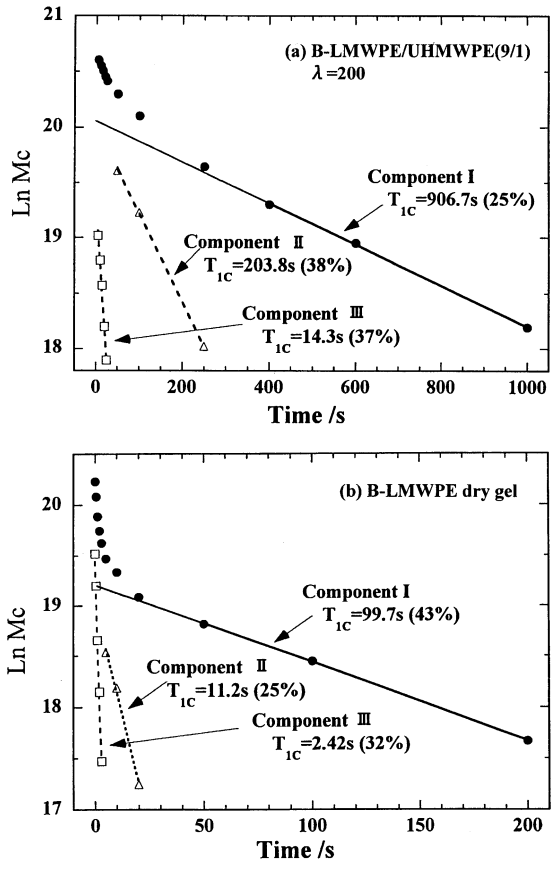

Fig. 13. Semi-logarithmic plot of the peak intensity of the orthorhombic component as a function of decay time obtained for: (a) B-LMWPE–UHMWPE (9/1) blends; (b) B-LMWPE dry gels.

G201 obtained elsewhere [30]. The mass fractions cannot be discussed from the CP/MAS spectra quantitatively but the spectrum indicates the existence of several components such as orthorhombic crystal form, monoclinic crystal form, interfacial state and rubbery state [31–33]. The peak intensity at 31 ppm shows that the non-crystalline component within UHMWPE films is much smaller than that within B-LMWPE–UHMWPE blend films. The spectrum of B-LMWPE–UHMWPE blend indicates a small increase in crystallinity with increasing draw ratio up to $\lambda = 200$, which is in good agreement with the results shown in Table 4.

Fig. 13 shows the variation of the relative intensity of orthorhombic crystal form measured by Torchia's pulse sequence [20] as a function of decay time τ for the B-LMWPE–UHMWPE (9/1) with $\lambda = 200$ and B-LMWPE dry gels. Peak deconvolution was carried out on each partially relaxed spectrum due to the overlapping peaks in Fig. 12. It is obvious that all T_{1C} decay curves in Fig. 13 exhibit overlapped exponential decay behavior. The initial slope of each decay curve yields a value of T_{1C}. The corresponding three T_{1C} values of the orthorhombic crystal within each specimen were obtained by least-squares fitting of the decay curves. As shown in Fig. 13(b), the orthorhombic crystals within the B-LMWPE (G808) films have no decay time beyond 100 s, as has been confirmed for PE (G201) film [30]. Namely, the longest T_{1C} of the orthorhombic crystal of B-LMWPE (G808) is shorter than that (145 s) of the PE (G201) melt film [30]. For the 9/1 blend, the longest T_{1C}, 906.7 s, corresponds to the orthorhombic crystals of UHMWPE and the value, 203.8 s, corresponds to that of B-LMWPE. In accordance with the previous result [30], the longest T_{1C} of orthorhombic crystals within UHMWPE homo-polymer film with $\lambda = 300$ reached 3463 s but the value within the 9/1 blend is much shorter. This indicates that the UHMWPE crystallites within the blend are in more unstable state containing dislocation and/or takes smaller size than crystallites within the UHMWPE homo-polymer film. If this is the case, the drastic decrease in the diffraction intensity from the (002) plane with temperature, as shown in Fig. 11, is attributed to the existence of unstable UHMWPE crystallites.

The background of this attempt is based on the concept that B-LMWPE–UHMWPE blend solution causes drastic decrease in solution viscosity in comparison with UHMWPE solution and then causes the promotion of the high production rate. However, the present experiment was carried out only at a fixed concentration of 0.4 g/100 ml of UHMWPE and the additional introduction of B-LMWPE was done to prepare blends with various compositions. The important factor is the relationship between viscosity of solution and mechanical property of the resultant drawn films. In doing so, a lot of efforts must be done by using a number of films prepared by gelation/crystallization from

solutions with various concentrations with B-LMWPE and UHMWPE.

4. Conclusion

B-LMWPE was blended with UHMWPE in solution using decalin as solvent, in which UHMWPE concentration was fixed to be 0.4 g/100 ml against solvent. The dry blend gels have the ability to form uniform films and the films can be elongated to more than 200-fold, even when B-LMWPE content reaches 90% of total polymer amount. The ultra-drawing mechanism was investigated by using DSC, WAXD and SAXS measurements. B-LMWPE and UHMWPE were crystallized independently because of different speeds of crystallization between B-LMWPE and UHMWPE under the gelation process. The greatest drawability was attributed to the long molecular chains of UHMWPE forming large crystal lamellae with high orientation on the film surface and keeping a suitable number of entanglements between the crystal lamellae. These entanglements ensured the smooth transition of the UHMWPE crystallites from a folded to a fibrous type by transmitting the drawing force as intermolecular cross-links. In this process, large amount of B-LMWPE is independent of the greatest drawing behavior of UHMWPE, since the UHMWPE and B-LMWPE chains with different crystallization speeds were crystallized separately and the both crystallites were isolated within the blend. In contrast, L-LMWPE–UHMWPE blend films could not be elongated up to five times. This was found to be due to the simultaneous crystallization under gelation process. This means that the co-crystallization hampered the ultra-drawing of UHMWPE crystallites.

References

[1] Zwijnenburg A, Pennings AJ. J Colloid Polym Sci 1976;254:868.
[2] Smith P, Lemstra PJ, Booij HC. J Polym Sci, Polym Phys Ed 1981;19:877.
[3] Matsuo M, Manley RSJ. Macromolecules 1982;15:985.
[4] Matsuo M, Manley RSJ. Macromolecules 1983;16:1505.
[5] Sawatari C, Okumura T, Matsuo M. Polym J 1986;18:741.
[6] Kanamoto T, Tsuruta A, Tanaka K, Takeda M, Porter RS. Polym J 1983;15:327.
[7] Kanamoto T, Tsuruta A, Tanaka K, Takeda M, Porter RS. Macromolecules 1988;21:470.
[8] Uehara H, Nakae M, Kanamoto T, Zachariades AE, Porter RS. Macromolecules 1999;32:2761.
[9] Moonen JAHM, Roovers WAC, Meier RJ, Kip BJ. J Polym Sci, Polym Phys Ed 1992;30:361.
[10] Hsieh YL, Hu XP. J Polym Sci, Polym Phys Ed 1997;35:263.
[11] Matsuo M, Inoue K, Abuymiya N. Sen-i-Gakkaishi 1984;40:275.
[12] Yeh J, Wu H. Polym J 1998;30:1.
[13] Sawatari C, Okumura T, Matsuo M. Polym J 1986;18:741.
[14] Mihailov M, Minkova L. Colloid Polym Sci 1987;265:681.
[15] Sawatari C, Matsuo M. Polymer 1989;30:1603.
[16] Bin Y, Fukuda M, Kurosu H, Matsuo M. Macromol Symp 2000;147:1.
[17] Mandelkern L. Rubber Chem Technol 1959;32:1392.
[18] Matsuo M, Sawatari C, Ohhata T. Macromolecules 1988;21:1317.
[19] Ogita T, Kawahara Y, Nakamura R, Ochi T, Minagawa M, Matsuo M. Macromolecules 1993;26:4646.
[20] Torchia DA. J Magn Reson 1981;44:117.
[21] Darras D, Sequela R, Rietsch F. J Polym Sci, Polym Phys Ed 1992;30:349.
[22] Matsuo M, Kitayama C. Polym J 1985;17:479.
[23] Ogita T, Yamamoto R, Suzuki N, Ozaki F, Matsuo M. Polymer 1991;32:822.
[24] Matsuo M, Sawatari C, Iida M, Yuneda M. Polym J 1985;17:1197.
[25] Blundel DJ. Acta Crystallogr 1970;A26:472.
[26] Hashimoto T, Shibayama M, Kawai H. Macromolecules 1980;13:1237.
[27] Glotin M, Mandelkern L. Colloid Polym Sci 1982;260:182.
[28] Domzy RC, Glotin M, Mandelkern L. J Polym Sci, Polym Symp 1984;71:151.
[29] Sawatari C, Matsuo M. Colloid Polym Sci 1985;263:783.
[30] Shimizu Y, Harashina Y, Sugiura Y, Matsuo M. Macromolecules 1995;28:6889.
[31] Ando I, Sorita T, Yamanobe T, Komoto T, Sato H, Deguchi K, Imanari M. Polymer 1985;26:1864.
[32] Earl WL, VanderHart DL. Macromolecules 1979;12:762.
[33] VanderHart DL. J Chem Phys 1976;64:830.